Inelastic photoproduction of J/ψ and Υ by gluons

Edmond L. Berger and D. Jones
High Energy Physics Division, Argonne National Laboratory, Argonne, Illinois 60439
(Received 17 November 1980)

Amplitudes are derived for the quantum-chromodynamic subprocess $\gamma g \to (J/\psi)g$, with a specific wave function used to represent the J/ψ as a $c\bar{c}$ system. The results are used to obtain the normalized total cross section σ_γ for the inelastic process $\gamma N \to (J/\psi)X$, predictions for the z and p_T dependence of inelastic J/ψ photoproduction, and predictions for the J/ψ helicity. The predictions apply as well to electroproduction at small Q^2.

I. INTRODUCTION

Considerable attention has been devoted to quantum-chromodynamic (QCD) predictions for $c\bar{c}$ charmed-quark production in high-energy processes.[1] Perturbative QCD computations are based on the assumption that the strong coupling parameter α_s is relatively small at the charm-quark mass scale. In photoproduction and electroproduction reactions, $\gamma N \to c\bar{c}X$, a popular approach is the "photon-gluon-fusion mechanism."[2,3] The incident γ interacts with the gluon content of the target via the subprocess $\gamma g \to c\bar{c}$, resulting in the production of bare c and $\bar{c}$ quarks. Estimates for hidden heavy flavor, and, in particular J/ψ production, are obtained from the $\gamma g \to c\bar{c}$ rate by supplementing the QCD cross section with qualitative notions based on "semilocal duality."[3] While it is successful phenomenologically in fitting selected data, several aspects of this approach have been questioned.[4]

In this paper we focus on inelastic J/ψ photoproduction and electroproduction at low Q^2: $\gamma N \to (J/\psi)X$. We study the amplitudes for the $2 \to 2$ QCD subprocess $\gamma g \to (J/\psi)g$, where g denotes a gluon. Our basic diagram is sketched in Fig. 1(a) along with its partners required by gauge invariance. The diagrams shown in Fig. 1 represent the simplest QCD process through which the initial γg interaction can lead to a color-singlet $(c\bar{c})$ state. One gluon in the final state carries off the color charge. In principle, additional gluons could be emitted in the reaction. However, *in the inelastic region* where $z = E_J/E_\gamma \leq 0.9$, we show that both the initial and final gluons in Fig. 1 are "hard." Arguments based on asymptotic freedom then suggest that the contributions from the higher-order multiple-gluon diagrams can be ignored with respect to Fig. 1.

In our approach the J/ψ is represented by a definite wave function, such that the final $c\bar{c}$ system in Fig. 1 is a color-singlet $J^P = 1^-$ state of specified mass. Absolute normalization is provided by the leptonic width Γ^J_{ee} of the J/ψ. The amplitude is free from infrared singularities. We argue that the process $\gamma N \to (J/\psi)X$ probes the gluon distribution in the nucleon at a momentum scale specified by the momentum transfer t from the γ to J/ψ. Although our results are presented here for J/ψ production, they apply equally well to any other $J^P = 1^-$ bound state of a heavy-quark–antiquark pair. We present predictions for the z and p_T variations of the inclusive yield $E\,d\sigma/d^3p$ in $\gamma N \to (J/\psi)X$, and predictions for the J/ψ-spin dependence of the cross section. Our approach differs substantially from previous work in that we incorporate proper spin and color constraints, as well as absolute normalization.[1-5] Comparison of our predictions with forthcoming inelastic data in the region

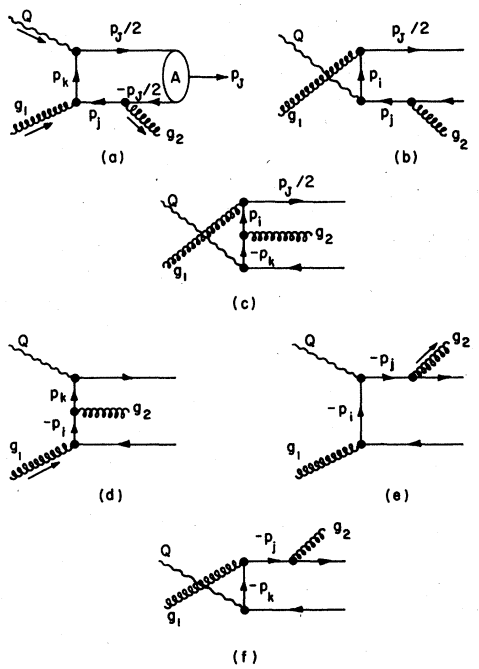

FIG. 1. The six diagrams for the subprocess $\gamma g_1 \to (J/\psi)g_2$. Momentum labels are indicated. The quark lines carrying momenta p_i, p_j, and p_k are all off-shell, whereas the lines carrying $p_J/2$ are on-shell.

$z \leq 0.9$ should provide an excellent test of first-order perturbative QCD.

In Sec. II, we discuss our description of the J/ψ as a bound color-singlet $J^P = 1^-$ system of a c and $\bar{c}$ quark, and we present explicit amplitudes for the QCD subprocess $\gamma g \to (J/\psi)g$. Differential cross sections are also obtained for this subprocess. These are normalized to the J/ψ electronic width Γ^J_{ee}. In Sec. III , we discuss the inclusive inelastic reaction $\gamma N \to (J/\psi)X$. We provide predictions for the normalization and energy dependence of the integrated yield, σ_γ, and present predictions for z and p_T dependences of the inclusive J/ψ yield, $E\, d\sigma/d^3p$. In Sec. IV, we provide predictions for the J/ψ-spin dependence of the inclusive yield. Conclusions, comparisons with available data, and some discussion are collected in Sec. V, including remarks on the expected rates for the ψ' and Υ.

II. THE SUBPROCESS $\gamma g \to (J/\psi)g$

It is generally accepted that the J/ψ is principally a bound system of a charm quark c and its antiquark $\bar{c}$. The photoproduction of J/ψ in $\gamma N \to (J/\psi)X$ thus involves the excitation of a $c\bar{c}$ system during the reaction process. Various mechanisms have been discussed in the literature, including the popular vector-dominance scheme[6] and the photon-gluon-fusion mechanism.[2,3] The mechansim which we propose has some features in common with the latter. Indeed both involve the interaction of the incident γ with the gluonic content of the nucleon target. However, in our approach, based on the subprocess $\gamma g \to (J/\psi)g$, an explicit normalized $J^P = 1^-$ wave function is used to represent J/ψ, and color balance is enforced explicitly. In this section, we first describe our representation of the J/ψ as a $c\bar{c}$ system, and then we present explicit amplitudes for $\gamma g \to (J/\psi)g$.

A. The J/ψ

As in several calculations[7] based on QCD, we ignore binding energy to leading order and treat the J/ψ as an S-wave $(c\bar{c})$ system with each spin-$\frac{1}{2}$ constituent carrying one half the mass and one half the four-momentum of the J/ψ. Thus, $m_c^{\text{eff}} = \frac{1}{2}m_J \equiv m_c$. The three helicity states of a $J^P = 1^-$ antifermion-fermion pair are represented easily in terms of charm-fermion spinors as follows:

$$v(\uparrow)\bar{u}(\uparrow) = \frac{1}{\sqrt{2}} \not{\epsilon}(\uparrow) \frac{\not{p}_J + m_J}{2}, \tag{2.1a}$$

$$v(\downarrow)\bar{u}(\downarrow) = \frac{1}{\sqrt{2}} \not{\epsilon}(\downarrow) \frac{\not{p}_J + m_J}{2}, \tag{2.1b}$$

and

$$\frac{1}{\sqrt{2}} [v(\uparrow)\bar{u}(\downarrow) + v(\downarrow)\bar{u}(\uparrow)] = \frac{1}{\sqrt{2}} \not{\epsilon}(0) \frac{\not{p}_J + m_J}{2}. \tag{2.1c}$$

The coupling strength of the J/ψ to $c\bar{c}$ is specified in terms of an overall constant A which is related to the value of the orbital wave function at the origin in momentum space. Thus, a J/ψ state of helicity h is represented in the amplitude by $AN_h \Sigma_{\lambda_i} v_{\lambda_1}(-p_J/2)\bar{u}_{\lambda_2}(p_J/2)$, where $\lambda_1 + \lambda_2 = h$, and N_h is the appropriate normalization constant: i.e., $N_{\pm 1} = 1$ and $N_0 = 1/\sqrt{2}$. The constant A may in turn be expressed in terms of the electronic width Γ^J_{ee} of the J/ψ.

To illustrate the above remarks and to obtain an explicit expression for the constant A, we present a calculation of Γ_{ee}. The relevant diagram is sketched in Fig. 2(a). Its corresponding amplitude is

$$M_{J \to e^+e^-} = AF_c e_q \left(\frac{1}{m_J^2}\right) \mathrm{Tr} \left(\frac{1}{\sqrt{2}} \not{\epsilon}_J \frac{\not{p}_J + m_J}{2} \gamma_\mu\right) L_\mu . \tag{2.2}$$

The color factor $F_c = \sqrt{3}$, e_q is the quark charge and L_μ denotes the $\gamma^* e^+ e^-$ vertex. It is easy to reduce Eq. (2.2) to

$$M_{J \to e^+e^-} = \sqrt{6} A e_q \epsilon_\mu L_\mu / m_J , \tag{2.3}$$

from which one may derive

$$\Gamma^J_{ee} = \frac{A^2 e_q^2 e^2}{2\pi m_J} . \tag{2.4}$$

The total *hadronic* width Γ^J_h of the J/ψ may also be computed from the three-gluon diagram sketched in Fig. 2(b), in which the J/ψ is again expressed in terms of Eqs. (2.1) and the constant A. These first-order QCD computations lead to the expression[7]

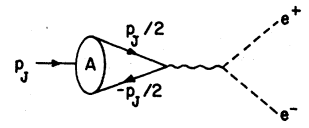

(a)

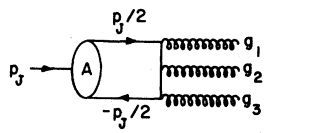

(b)

FIG. 2. (a) Diagram for the decay $J \to e^+e^-$. (b) Sketch of the process $J \to 3g$.

$$\Gamma_h^J/\Gamma_{ee}^J=\frac{5}{18}\frac{\pi^2-9}{\pi}\frac{\alpha_s^3}{\alpha^2}. \tag{2.5}$$

The strong coupling parameter α_s is to be evaluated at a momentum scale typical of m_J^2 or of m_c^2. Experimentally the ratio in Eq. (2.5) is close to 10, yielding $\alpha_s\simeq 0.2$. Although higher-order QCD corrections to Eq. (2.5) may not be small,[8] we are encouraged by the fair agreement of Eq. (2.5) with experiment. In our amplitude for $\gamma g\to(J/\psi)g$, one of the gluons in Fig. 2(b) is replaced by a photon. The reasonable agreement of the first-order result in Eq. (2.5) with data suggests that our overall rate for $\gamma g\to(J/\psi)g$ should also not be far off the mark.

B. Amplitudes for $\gamma g\to(J/\psi)g$

The six diagrams which form a gauge-invariant set for $\gamma g\to(J/\psi)g$ are sketched in Fig. 1. Momentum labels are indicated, but color labels are omitted in Fig. 1 because all six amplitudes are proportional to the same color factor,

$$F_c=\frac{1}{2\sqrt{3}}\delta_{ab}, \tag{2.6}$$

where a is the color index for the final gluon, and b is the index for the initial gluon.

The quark lines which carry momentum $p_J/2$ are on-shell, whereas the lines carrying momenta p_i, p_j, and p_k are off-shell. The initial and final gluons are on-shell: $g_1^2=0$, $g_2^2=0$. The final gluon g_2 may become "soft" only at the subprocess threshold, $s=m_J^2$, as we show explicitly below. However, in the inelastic domain, $z<0.9$, g_2 is always hard. The charm-quark mass is $m_c^{\text{eff}}=\frac{1}{2}m_J\equiv m_c$.

1. Kinematics

We define variables s, t, and u for the subprocess as

$$s=(Q+g_1)^2=(p_J+g_2)^2,$$

$$t=(p_J-Q)^2=(g_2-g_1)^2, \tag{2.7}$$

and

$$u=(p_J-g_1)^2=(g_2-Q)^2.$$

In terms of these variables,

$$p_k^2-m_c^2=(\tfrac{1}{2}p_J-Q)^2-m_c^2=\tfrac{1}{2}(t-m_J^2), \tag{2.8}$$

$$p_j^2-m_c^2=(\tfrac{1}{2}p_J+g_2)^2-m_c^2=\tfrac{1}{2}(s-m_J^2), \tag{2.9}$$

and

$$p_i^2-m_c^2=(\tfrac{1}{2}p_J-g_1)^2-m_c^2=\tfrac{1}{2}(u-m_J^2). \tag{2.10}$$

We note that the kinematic limits on s, t, and u are $m_J^2\le s\le s_T$, $0\ge t\ge-(s-m_J^2)$, and $0\ge u\ge-(s-m_J^2)$. The total energy $s_T=(Q+p_N)^2$. We ignore the nucleon mass.

The traditional variables z and p_T^2 may also be employed. Here z is defined as

$$z=\frac{p_J\cdot p_N}{Q\cdot p_N}, \tag{2.11}$$

and p_T is the transverse momentum of the J/ψ with respect to Q. In the laboratory frame of reference $z=E_J/E_\gamma$. In terms of z and p_T^2,

$$s-m_J^2=\frac{m_J^2(1-z)}{z}+\frac{p_T^2}{z(1-z)}. \tag{2.12}$$

The overall energy constraint restricts the combination of p_T^2 and z because

$$m_J^2\le\frac{m_J^2}{z}+\frac{p_T^2}{z(1-z)}\le s_T. \tag{2.13}$$

The strong coupling strength α_s of the initial gluon g_1 in Fig. 1 is well defined since g_1 couples to quark lines which are always off-shell by at least $\frac{1}{2}m_J^2$. As $s\to m_J^2$, both quarks to which g_2 couples are on-shell in Fig. 2(a); thus α_s for this vertex may be ill-defined as $s\to m_J^2$. This is the only potential danger point in phase space. Our amplitude is expressly finite in this infrared limit, but this practical advantage does not remove all concerns about the physical applicability of our answer for $s\to m_J^2$. Indeed as $s\to m_J^2$, diagrams with multiple soft-gluon emissions may become competitive with our Fig. 1. However, if we confine our interest to the *inelastic domain*, $z<1$, Eq. (2.12) shows that we are able to restrict the difference $s-m_J^2=2(p_j^2-m_c^2)$ to strictly positive values. We shall return to this issue again in Sec. III A. Our conclusion is that for $z<0.9$, g_2 is a "hard" gluon, and the results of our calculation should therefore be a valid first-order perturbative estimate of the *inelastic* cross section.

2. Invariant amplitudes and cross section

Inspection of the diagrams in Fig. 1 shows that the amplitudes occur in pairs, with $M_a=M_f$, $M_b=M_e$, and $M_c=M_d$. Therefore, the total amplitude

$$M=2AF_c e_q g^2(M_{(a)}^{\mu\beta\alpha}+M_{(b)}^{\mu\beta\alpha}+M_{(c)}^{\mu\beta\alpha})\epsilon_\mu(Q)\epsilon_\beta(g_1)\epsilon_\alpha(g_2). \tag{2.14}$$

Our explicit expression for $M_{(a)}$ is

$$M_{(a)}^{\mu\beta\alpha}=\frac{4}{\sqrt{2}}\,\mathrm{Tr}\left[\not\epsilon_J(\not p+m_c)\gamma_\mu\frac{(\not p-\not Q)+m_c}{(t-m_J^2)}\gamma_\beta\times\frac{(-\not p-\not g_2)+m_c}{(s-m_J^2)}\gamma_\alpha\right]. \tag{2.15}$$

For convenience we have introduced $p=\frac{1}{2}p_J$. Our amplitude Eq. (2.14) satisfies the gauge-invariance requirement whereby $M\to 0$ if any one of the $\epsilon_\delta(V)$ in Eq. (2.14) is replaced by V_δ.

We may sum over the spins of the initial photon and over the gluon spins by employing substitutions

$$\sum \epsilon_\mu(V)\epsilon_\nu(V)\to -g_{\mu\nu}. \tag{2.16}$$

To sum over the J/ψ spin states, we use

$$\sum \epsilon_J^\delta \epsilon_J^{\delta'} \to -g_{\delta\delta'}+\frac{p_J^\delta p_J^{\delta'}}{m_J^2}. \tag{2.17}$$

After summing over the spins of the final gluon and the J/ψ and averaging over the spins of the photon and initial gluon, we obtain

$$\overline{\sum_{\text{spins}}} |M|^2 = 64g^4 e_q^2 m_J^2 A^2 F_c^2 \times \frac{s^2(s-m_J^2)^2+t^2(t-m_J^2)^2+u^2(u-m_J^2)^2}{(s-m_J^2)^2(t-m_J^2)^2(u-m_J^2)^2}. \tag{2.18}$$

The average over initial gluon colors and sum over final gluon colors replaces F_c^2 with $F_c^2 = \frac{1}{12}$.

The differential cross section $d\sigma/dt$ for the subprocess is

$$\frac{d\sigma}{dt}=\frac{1}{16\pi s^2}\overline{\sum_{\text{spins, color}}}|M|^2. \tag{2.19}$$

III. $\gamma N\to(J/\psi)X$

In this section we present and discuss the contribution of the QCD subprocess $\gamma g\to(J/\psi)$ to the cross section for $\gamma N\to(J/\psi)X$.

A. Applicable region of phase space

It seems necessary to establish first the region of phase space in which we believe our results may be applicable. We begin with a discussion based on Fig. 3. Whatever the nature of the upper vertex ($\gamma\to J/\psi$) in Fig. 3, the invariant mass of the recoil system X must be large enough to justify use of a parton basis rather than a hadron basis. If m_X is too small, specific hadronic exclusive channels will probably be important in the data. In particular, the elastic process $\gamma N\to(J/\psi)N$ is known to provide a significant fraction of the observed cross section.[9,10] The description of this elastic process and of N^* production is not included in our Fig. 3 even in an average sense. The proper computation of the elastic process $\gamma N\to(J/\psi)N$ would require use of a diagram in which coherence effects necessary to reconfigure the final momenta into a nucleon wave function would be manifest. Consequently, we believe that the $\gamma g\to(J/\psi)g$ contribution is applicable only when $m_X>W_0$. In deep-inelastic processes, such as $\nu N\to\mu X$, similar considerations restrict the usual parton description to $m_X^2\equiv W^2>W_0^2$. In practice, W_0 is chosen such that $W_0\geq 2$ GeV.

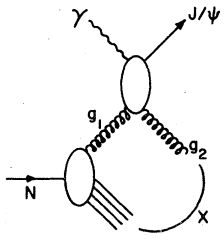

FIG. 3. Parton-model diagram for $\gamma N\to(J/\psi)g_2X'$ in which the subprocess is $\gamma g_1\to(J/\psi)g_2$.

In deep-inelastic processes, the constituent densities are probed at a momentum scale specified by the Q^2 of the virtual γ, Z, or W. The validity of the parton approach is restricted to values of $Q^2(\geq Q_0^2)$ large enough to justify the impulse approximation. In our problem, the analog of Q^2 is the momentum transfer $t=(p_J-Q)^2$, and $\gamma N\to(J/\psi)X$ probes the gluon density $G(x,t)$ in the nucleon at momentum scale $|t|$.

The restriction of the region of applicability of our results to $m_X>W_0$ and to $|t|>Q_0^2$ may be phrased in terms of the variables z and p_T^2 introduced in Sec. II. We begin by noting that

$$m_X^2=[g_2+(1-x)p_N]^2\equiv\left[g_2+\frac{(1-x)}{x}g_1\right]^2 = -\frac{(1-x)}{x}t. \tag{3.1}$$

Here x is the fraction of the incident nucleon momentum carried by the gluon g_1. Furthermore,

$$x=\frac{s}{s_T}=\frac{1}{s_T}\left[\frac{m_J^2}{z}+\frac{p_T^2}{z(1-z)}\right] \tag{3.2}$$

and

$$t=-(1-z)s. \tag{3.3}$$

At large total energy s_T, the restriction $m_X>W_0$ therefore becomes the statement

$$(1-z)>\left(\frac{p_T^2+W_0^2}{s_T}\right), \tag{3.4}$$

and z is bounded away from 1 even at $p_T^2=0$.

According to Eqs. (3.2) and (3.3), the restriction $|t|>Q_0^2$ requires

$$(1-z)>\frac{Q_0^2-p_T^2}{Q_0^2+m_J^2}. \tag{3.5}$$

Although not rigorously justified, it is common

to trust QCD calculations down to values of $Q_0^2 \simeq 1$ GeV^2. Using this value of Q_0^2 in Eq. (3.5), we determine that our results should apply for $z \leq 0.9$.

B. Cross sections

We obtain the cross section $d\sigma/dt$ for $\gamma N \to (J/\psi)N$ by convoluting Eq. (2.19) with the gluon density in the nucleon, $G(x)$. We shall ignore the expected evolution of $G(x,t)$ with t. This evolution could be included or even extracted from the J/ψ data in a more refined analysis:

$$\frac{d\sigma}{dt}(\gamma N \to J/\psi X) = B m_J^4 \int G(x)dx f(s,t), \tag{3.6}$$

$$B = \frac{8\pi\alpha_s^2 \Gamma_{ee}^J}{3\alpha m_J}, \tag{3.7}$$

$$f(s,t) = \frac{1}{s^2}\left[\frac{s^2(s-m_J^2)^2 + t^2(t-m_J^2)^2 + u^2(u-m_J^2)^2}{(s-m_J^2)^2(t-m_J^2)^2(u-m_J^2)^2}\right], \tag{3.8}$$

$$s + t + u = m_J^2, \tag{3.9}$$

and

$$s = x s_T. \tag{3.10}$$

The overall bounds on x are such that

$$\frac{m_J^2}{s_T} \leq x \leq 1. \tag{3.11}$$

Because we use a gluon density, $G(x)$, which is independent of t, the integral over t may be done analytically, and we obtain

$$\frac{d\sigma}{dx} = B m_J^4 G(x) I(x), \tag{3.12}$$

where

$$I(x) = \frac{2}{(s+m_J^2)^2}\left[\frac{s-m_J^2}{s m_J^2} + \frac{2}{s+m_J^2}\ln(s/m_J^2)\right] + \frac{2(s+m_J^2)}{s^2 m_J^2 (s-m_J^2)} - \frac{4\ln(s/m_J^2)}{s(s-m_J^2)^2}. \tag{3.13}$$

We note that $I(x)$ is finite at all s, even in the infrared limit $s \to m_J^2$.

In our numerical work, we adopt the simple form

$$xG(x) = 3(1-x)^5 \tag{3.14}$$

suggested by counting rules and momentum constraints.[11] We also adopt the effective constant value $\alpha_s = 0.3$, and we use $\Gamma_{ee}^J = 4.8$ keV. Integrating Eq. (3.12) over x, we obtain the inelastic photoproduction cross section σ_γ vs E_γ shown in Fig. 4. The cross section rises rapidly from threshold, with a derivative controlled by the large-x behavior of Eq. (3.14). As $s_T \gg m_J^2$, the curve reaches an approximate plateau value determined by the $x \to 0$ behavior of $G(x)$. With the simple form we employ for $xG(x)$, and with constant α_s, the asymptotic value of σ_γ is 8.8 nb. An explicit analytic evaluation of $\sigma_\gamma(s_T)$ is presented in Appendix A.

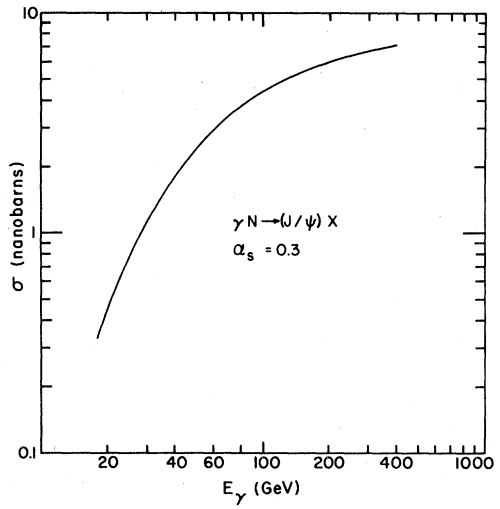

FIG. 4. Shown is our prediction for the inelastic cross section σ_γ versus E_γ for direct production of the J/ψ in $\gamma N \to (J/\psi)X$. To obtain this result we used $\alpha_s = 0.3$. The prediction is proportional to α_s^2, and therefore the choice of a larger value of α_s would increase σ_γ significantly.

As yet there are no published data which may be compared directly with our Fig. 4. There are two sources of inelasticity which contribute to the present sample of inelastic data[10] on $\mu N \to \mu'(J/\psi)X$ at low Q^2. In these data[10] inelasticity (i.e., $z_J < 1$) may arise either from "true" inelasticity at the hadron vertex, which we calculate, or as a consequence of elastic or quasielastic production of the ψ' or other charmonium states, with a subsequent cascade such as $\psi' \to (J/\psi)\pi\pi$. The resolution of the experiment is such that the two effects cannot be isolated. Using three different indirect methods of analysis, the experimenters conclude that about half of their inelastic J/ψ events can be accounted for by production and decay of charmonium states above the J/ψ. They do not state the energy, ν, dependence of this fraction.

At $\nu = 100$ GeV, the measured inelastic cross section[10] is in the neighborhood of 12 nb. If we assign half of this to the cascade effects, then our predicted inelastic yield of 4.5 nb at 100 GeV is close to reality. At higher energies, however, the inelastic cross section[10] rises much beyond our expectations. Indeed at $\nu \simeq 400$ GeV, $\sigma_{\text{exp}} \simeq 40$

nb and the cascade fraction would have to be 75% in order for theory and experiment to agree. For the moment we prefer to withold judgment, pending more definitive data. As discussed below, the theoretical z and p_T distributions agree fairly well with the shape of the data. Higher-order QCD corrections to the ratio $\sigma_\gamma/\Gamma_{ee}$ may not be negligible, and should be computed eventually.

The appropriate value of α_s to be used in our Eq. (3.7) is also uncertain, and our choice of $\alpha_s = 0.3$ may be conservatively low. If we adopt instead the value of α_s suggested by the four-flavor model and $\Lambda = 0.5$, we find the larger value $\alpha_s(m_J^2) = 6\pi/[25\ln(m_J/\Lambda)] \simeq 0.4$. Because σ_γ is proportional to α_s^2, use of this value of α_s increases σ_γ by the large factor 1.8.

A comparison of Fig. 4 with the published (primarily elastic) data[9] on $\gamma N \to (J/\psi)X$ and on $\mu N \to \mu'(J/\psi)X$ at $Q^2 = 0$ shows that our inelastic curve rises more rapidly with energy and reaches its plateau at a higher value of E_γ than is true of the elastic data.

C. Distribution in z and p_T^2

It is useful to reexpress our cross sections in the form of the inclusive yield $E\,d\sigma/d^3p$ of the J/ψ as a function of z and p_T^2. We obtain

$$\frac{E\,d\sigma}{d^3p} = \frac{xG(x)z^2(1-z)m_J^4 B}{\pi[m_J^2(1-z)+p_T^2]^2}\bar{f}(z,p_T^2), \tag{3.15}$$

with

$$\bar{f}(x,p_T^2) = \frac{1}{(m_J^2+p_T^2)^2} + \frac{(1-z)^4}{[p_T^2+m_J^2(1-z)^2]^2} + \frac{z^4 p_T^4}{(m_J^2+p_T^2)^2[p_T^2+m_J^2(1-z)^2]^2}. \tag{3.16}$$

The value of B if provided by Eq. (3.7), and x is related to z and p_T^2 through Eq. (3.2). Note that $E\,d\sigma/d^3p = z\,d\sigma/\pi\,dz\,dp_T^2$.

We remark that our cross section $d\sigma/dz\,dp_T^2$ is well behaved as $p_T^2 \to 0$. Equation (3.15) appears to be singular at $z = 1$ if $p_T^2 = 0$. Nevertheless, the cross section is finite at this point, and the point $z = 1$ is excluded from our region of interest according to the discussion in subsection A, Eq. (3.4). Finiteness is guaranteed by the total energy constraint whereby the allowed range in p_T^2 vanishes as $z \to 1$. Indeed,

$$0 \le p_T^2 \le z(1-z)s_T - m_J^2(1-z). \tag{3.17}$$

The interested reader may easily evaluate Eq. (3.15) for arbitrary values of E_γ, z, and p_T^2. We restrict our numerical presentation to a display of $d\sigma/dz$ integrated over p_T^2, and to $d\sigma/dp_T^2$ vs p_T^2 for selected values of $z < 0.9$.

In Fig. 5, we provide the cross section $d\sigma/dz$ vs z for three values of the incident photon energy

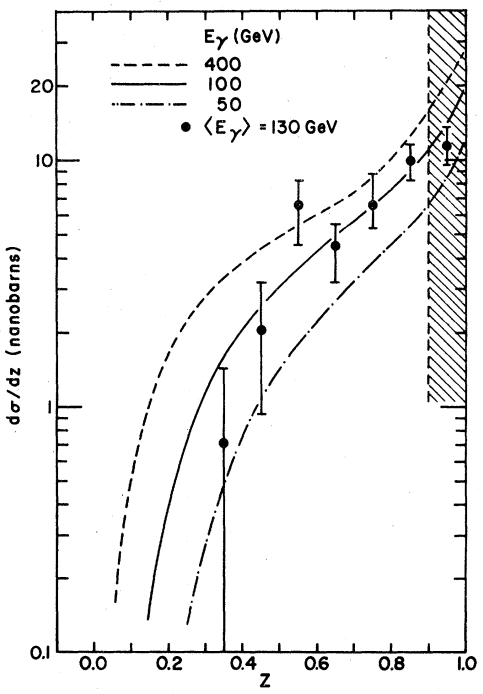

FIG. 5. The distribution $d\sigma/dz$ is predicted for $E_\gamma = 50$, 100, and 400 GeV. The region $z > 0.9$ is excluded from the range of validity of the model. Data points are from the CERN-EMC collaboration (Ref. 10) for the process $\mu N \to \mu'(J/\psi)X$ at $\langle Q^2\rangle \cong 4$ GeV^2 and $\langle E_\gamma\rangle \simeq 130$ GeV. The data are plotted with arbitrary normalization relative to our normalized predictions.

E_γ. The curves show a pronounced peak near $z = 1$. However, at all three energies, at least 65% of the cross section is in the region $z \le 0.9$, and this fraction increases with E_γ. Superimposed on Fig. 5 are data points from the CERN–European Muon Collaboration (CERN-EMC) experiment[10] $\mu N \to \mu'(J/\psi)X$ at an average $\nu = E_\gamma = 130$ GeV. Because $\langle Q_\gamma^2\rangle \simeq 4$ GeV^2 in these data, the results are not directly comparable with our $Q^2 = 0$ predictions. If we assume that the effects of small (with respect to m_J^2) but nonzero Q^2 are insignificant, we may note that the z dependence of our curves agrees well with the trend of the data. In a subsequent paper we will treat $\mu N \to \mu'(J/\psi)X$ explicitly, and we shall provide detailed predictions for the Q^2 dependence.

In $\gamma N \to (J/\psi)X$, the transverse momentum of the J/ψ is balanced by that of the final gluon, g_2. In Fig. 6 we provide predictions for the mean values $\langle p_T\rangle$ and $\langle p_T^2\rangle$ vs z for three values of E_γ. We observe that the QCD process provides relatively large values of $\langle p_T\rangle$, in the neighborhood of $\langle p_T\rangle = 1$ GeV for $E_\gamma \simeq 100$ GeV. In confronting these expectations with data, one should recall that additional finite (intrinsic) $\langle k_T^2\rangle$ is presumably

supplied by the initial gluon, g_1. We have neglected this latter effect in our calculation. Adding the contributions in quadrature, we would expect

$$\langle p_T^2\rangle_{\rm exp} \simeq \langle k_T^2\rangle + \langle p_T^2\rangle_{\rm QCD}\,, \tag{3.18}$$

with the QCD value $\langle p_T^2\rangle_{\rm QCD}$ provided in Fig. 6.

Our distributions $E\,d\sigma/d^3p$ are plotted vs p_T^2 in Fig. 7 for five values of z, at $E_\gamma = 200$ GeV. Shown also are the available inelastic data from the EMC experiment.[10] These data are integrated over $z > 0.3$ but are predominantly from the large-z region, as shown in Fig. 5. The agreement is fine and should motivate a more detailed comparison. We note that at very large p_T^2, the curves fall off as p_T^{-8}.

Our inclusive yield can be reexpressed as a function of the scaling variables m_J^2/s_T and p_T^2/m_J^2. Specifically,

$$\frac{E\,d\sigma}{d^3p} = \frac{\alpha_s^2\Gamma_{ee}^J}{m_J^5} F\left(\frac{m_J^2}{s_T}, \frac{p_T^2}{m_J^2}, z\right). \tag{3.19}$$

The dependence on s_T arises through the definition of x, Eq. (3.2). Equation (3.19) allows us to conclude directly that $\langle p_T^2\rangle$ must grow linearly with s_T at fixed z and m_J^2/s_T:

$$\langle p_T^2\rangle_{\rm QCD} = s_T f_1(z, m_J^2/s_T)\,. \tag{3.20}$$

Moreover, we may apply our results to other heavy vector-meson states with mass m_V, such as the ψ' and members of the Υ family. Equation (3.19) permits an estimate Υ yields from our curves for J/ψ production. In particular, we deduce that

$$\langle p_T^2\rangle_{\rm QCD} = m_V^2 f_2\left(z, \frac{m_V^2}{s_T}\right). \tag{3.21}$$

The Υ states are expected to be produced with much larger values of $\langle p_T\rangle$ than the ψ states. We note that the relevant p_T variable in Eqs. (3.15) and (3.16) is not exactly the "transverse mass" $(m_V^2 + p_T^2)^{1/2}$. Instead, the vector-meson mass appears in the equations multiplied by powers of z and $1-z$.

IV. SPIN DEPENDENCE

Our amplitude, Eqs. (2.14) and (2.15), specifies a very definite spin alignment of the J/ψ which changes with p_T^2 and z. Before discussing our detailed results, we present a qualitative argument to indicate why spin effects are expected. In Fig. 1, the photon and gluon couplings conserve helicity. Thus, in the limit of massless quarks, the J/ψ would be forced to be in a state of helicity zero (i.e., $\sigma_T = 0$). Because the charm quarks are massive, helicity flip is possible, and $\sigma_T \propto m_c^2 \equiv \frac{1}{4}$

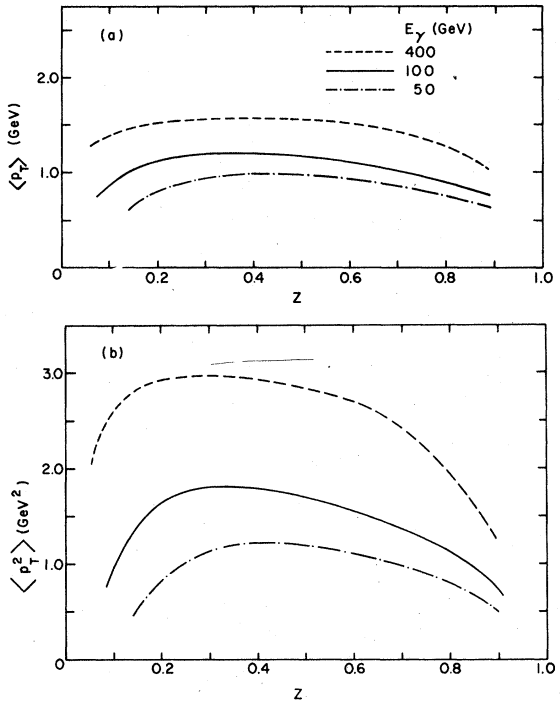

FIG. 6. Predictions for the variation with z of (a) $\langle p_T\rangle$, and (b) $\langle p_T^2\rangle$ for $\gamma N \to (J/\psi)X$ at $E_\gamma = 50$, 100, and 400 GeV.

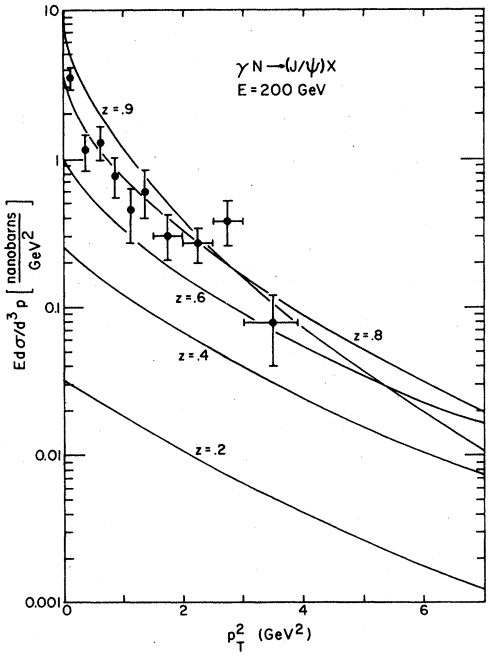

FIG. 7. The inclusive yield $E\,d\sigma/d^3p$ vs p_T^2 at $E_\gamma = 200$ GeV for five values of z. Data from Ref. 10 for inelastic J/ψ production are also shown. Normalization of these data relative to the theory curves is arbitrary. The data cover the range $z > 0.3$ but are concentrated primarily at large z.

m_J^2. The "dominant" longitudinal cross section σ_L is forced to vanish at $p_T = 0$ for obvious reasons associated with helicity conservation in the overall process $\gamma g \to Jg$. Thus, $\sigma_L \propto p_T^2$. Mild corrections to this statement are associated with nonzero values of $\langle k_T^2 \rangle$ which we have ignored.

It is most convenient to present our detailed results in terms of t-channel helicity states. This corresponds to selection of the incident γ direction as the axis of quantization. In the J/ψ rest frame, the cross section σ_T yields a distribution $d\sigma/d\cos\theta \propto (1+\cos^2\theta)$ for the decays $J/\psi \to \mu\bar{\mu}$ or $J/\psi \to e^+ e^-$. Here θ is the direction of an emerging lepton measured with respect to the direction of the incident γ, as seen in the J/ψ rest frame. Likewise, $\sigma_L \propto \sin^2\theta$.

To obtain σ_L and σ_T we choose specific representations for ϵ_J in Eq. (2.15), rather than summing over J/ψ spins as in Eq. (2.17). For σ_L, the J/ψ spin-summed result [Eq. (3.8)] is replaced by

$$f \to f_L(s,t) = \frac{2m_J^2 ut(s^2+u^2)}{s(s-m_J^2)^2(u-m_J^2)^2(t-m_J^2)^4}. \quad (4.1)$$

Since $\sigma = \sigma_L + \sigma_T$ the net J/ψ helicity-one (transverse) cross section may be obtained from Eqs. (3.8) and (4.1) by subtraction. Our ratio of the J/ψ helicity-zero cross section to the *total* cross section is expressed in terms of z and p_T^2 as

$$R = \frac{E\,d\sigma_L/d^3p}{E\,d\sigma/d^3p} = \frac{2z^2 p_T^2 m_J^2\{[m_J^2(1-z)+p_T^2]^2 + z^2 p_T^4\}}{(m_J^2+p_T^2)^2\{[m_J^2(1-z)^2+p_T^2]^2 + (1-z)^4(m_J^2+p_T^2)^2 + z^4 p_T^4\}}. \quad (4.2)$$

Equation (4.2) indicates that the J/ψ helicity-zero fraction of the inelastic cross section is at its largest at large z and modest p_T^2. For small z, $R \to 0$ as z^2. At large p_T, $R \propto p_T^{-2}$. In Fig. 8 we present a numerical evaluation of R as a function of p_T for various values of z.

We note that σ_L accounts for nearly one-half the total cross section at large values of z ($z > 0.8$) and intermediate values of p_T. In this part of phase space the J/ψ decay- angular distribution is therefore predicted to be nearly isotropic. A detailed examination of the J/ψ angular distributions in the present data[10] should provide a first test of our predictions.

V. DISCUSSION AND CONCLUSIONS

We have provided specific predictions based on parton-model perturbation theory for the inelastic photoproduction reaction $\gamma N \to (J/\psi)X$. As discussed in some detail in Sec. III A, these predictions should be applicable for $z = E_J/E_\gamma \leq 0.9$. Confrontation of these expectations with the data on the absolute rate, the z and p_T^2 dependences, and the spin dependence of the J/ψ cross section $E\,d\sigma/d^3p$ should provide a good test of the applicability of first-order QCD. We are aware that higher-order corrections to the rate for $J \to 3g$ may not be small.[8] We are interested in the possibility that such higher-order effects may also influence expectations for the crossed process $\gamma g \to Jg$. It is necessary to study the higher-order corrections to both the J/ψ wave function and the more strictly perturbative parts of Fig. 1. It may also be useful to examine the consequences of replacing our gluon density $G(x)$ with a form $G(x,t)$ which evolves with t in the manner suggested by QCD.

Our results apply only to *direct* inelastic production of the J/ψ. Some fraction of the J/ψ signal arises through a cascade process in which, e.g., a χ or ψ' state is produced directly and then $\chi \to (J/\psi)\gamma$. The two sources of inelasticity should be separated experimentally.

Inspection of Eqs. (3.6) and (3.11) shows that σ_γ is proportional to

$$\sigma_\gamma \propto \frac{\Gamma_{ee}^J}{m_J^3} F(s_T/m_J^2). \quad (5.1)$$

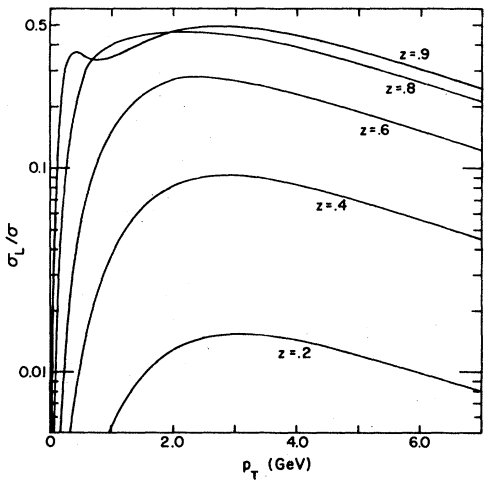

FIG. 8. The predicted ratio $R = (E\,d\sigma_L/d^3p)/(E\,d\sigma/d^3p)$ is shown as a function of p_T for various values of z. Here σ_L is the cross section for production of the J/ψ with t-channel helicity zero, and σ is the cross section summed over the J/ψ helicities.

In Eq. (5.1) we have ignored possible dependence of α_s on m_J^2 and s_T. Equation (5.1) permits the use of Fig. 4 to obtain estimates for the cross sections for inelastic photoproduction of the ψ' and Υ.

In particular, because $m_J/m_{\psi'} \simeq 0.84$, and $\Gamma_{ee}(\psi')/\Gamma_{ee}(J) \simeq 0.44$, we estimate that $\sigma_\gamma(\psi')/\sigma_\gamma(J) \simeq 0.26$ for values of $s_T \cong 2E_\gamma$ sufficiently above the region of the threshold rise in Fig. 4. Likewise, the asymptotic plateau height for $\sigma_\gamma(\Upsilon)$ should be roughly $0.32 \times \Gamma_{ee}^{\Upsilon}/\Gamma_{ee}^{J} \simeq 0.08$ nb. The present *upper limit*[12] on Υ production in $\mu N \to \mu' \Upsilon X$ exceeds our estimate.

In a paper now in preparation we will present detailed predictions for the electroproduction process $\mu N \to \mu'(J/\psi)X$ for all Q^2.

ACKNOWLEDGMENTS

We are pleased to acknowledge encouraging conversations with J. D. Bjorken and T. DeGrand. This work was performed under the auspices of the United States Department of Energy.

APPENDIX

In this appendix we give the analytic expression for the integrated yield σ_γ in the process $\gamma N \to \psi X$. In order to integrate Eq. (3.12), we eliminate s in favor of x via $s = xs_T$. Kinematical constraints then impose the restriction $x_{\min} = m_J^2/s_T$ so that

$$\sigma_\gamma = 2B \frac{x_{\min}^2}{m_J^2} I(x_{\min}), \tag{A1}$$

where

$$I(x_{\min}) = \int_{x_{\min}}^1 dx\, g(x, x_{\min}) \tag{A2}$$

and

$$g(x, x_{\min}) = \frac{G(x)}{x}\left[\frac{(x - x_{\min})}{(x + x_{\min})^2} + \frac{2x_{\min} x \ln x/x_{\min}}{(x + x_{\min})^3} + \frac{x + x_{\min}}{x(x - x_{\min})} - \frac{2x_{\min} \ln x/x_{\min}}{(x - x_{\min})^2}\right]. \tag{A3}$$

Note that the apparent end-point singularities in the last two terms of Eq. (A3) cancel, as expanding the logarithm in a power series will make obvious.

After straightforward but tedious integration, one finds

$$I(x_{\min}) = \frac{6}{x_{\min}^2}\left[H_1(x_{\min}) + H_2(x_{\min}) - \tfrac{5}{4}(1 - x_{\min})^5\right], \tag{A4}$$

where

$$H_1(x) = \left[\frac{\pi^2}{12} + \mathrm{Li}_2(-x) + \ln x \ln\frac{1+x}{\sqrt{x}}\right](1+x)^3(1 - 3x + 6x^2) + \frac{\ln^2 x}{2} - x \ln x\left[1 - \frac{x}{2} + 12x^2 + 6x^3\right] + (1 - x)\left[-\tfrac{3}{4} + \frac{x}{4} - \frac{27x^3}{2} - \frac{9x^4}{2}\right], \tag{A5}$$

$$H_2(x) = -\left[\mathrm{Li}_2(x) + \ln x \ln\frac{1-x}{\sqrt{x}} - \frac{\pi^2}{6}\right](1 - x)^4(2 + 3x) - \ln^2 x(1 - \tfrac{5}{2}x) - x \ln x(2 + 6x - \tfrac{17}{2}x^2 + 3x^3) + (1 - x)(-2 - \tfrac{47}{6}x^2 + \tfrac{137}{12}x^3 - \tfrac{49}{12}x^4), \tag{A6}$$

and $\mathrm{Li}_2(x)$ is the dilogarithm.[13] Although this form for $I(x)$ does not lead to any great enlightenment, it is convenient for numerical evaluation of the integrated yield. The asymptotic limit of σ_γ takes on a particularly simple form as $s_T \to \infty$ since then $x_{\min} \to 0$ and

$$\lim_{x \to 0} x^2 I(x) = \frac{5\pi^2 - 48}{2}. \tag{A7}$$

Thus the asymptotic limit of the integrated yield is given by

$$\sigma_{\gamma\,(s_T \to \infty)} = \frac{B}{m_J^2}(5\pi^2 - 48) = \frac{8\pi\alpha_s^2 \Gamma_{ee}^J}{3\alpha m_J^3}(5\pi^2 - 48). \tag{A8}$$

We call attention to the similarity of the factor $(5\pi^2 - 48)$ in this calculation and the factor $(5\pi^2 - 45)$ that arises in the ratio of the hadronic to electronic widths, Eq. (2.5). In each case, it is the difference of two large numbers that leads to the small final answer.

[1]For a recent review, see the article by R. J. N. Phillips, in *High Energy Physics—1980*, proceedings of the XXth International Conference, Madison, Wisconsin, 1980, edited by L. Durand and L. G. Pondrom (AIP, New York, 1981).

[2]L. Jones and W. Wyld, Phys. Rev. D 17, 2332 (1978); M. Glück and E. Reya, Phys. Lett. 79B, 453 (1978); 83B, 98 (1979); J. P. Leveille and T. Weiler, Nucl. Phys. B147, 147 (1979); Phys. Lett. 86B, 377 (1979); T. Weiler, Phys. Rev. Lett. 44, 304 (1980); V. Barger, W. Y. Keung, and R. J. N. Phillips, Phys. Rev. D 20, 630 (1979); Phys. Lett. 91B, 253 (1980); 92B, 179 (1980).

[3]H. Fritzsch and K. H. Streng, Phys. Lett. 72B, 385 (1978).

[4]In $\gamma g \to c\bar{c}$, the $(c\bar{c})$ system is not a color singlet, and cannot be in a $J^P = 1^-$ state. Color must be shed, and the J^P of the $(c\bar{c})$ system must change before a J/ψ can emerge. Presumably this is achieved through soft-gluon emission, but in an unspecified way. Via semilocal duality, a spread of masses of the $(c\bar{c})$ pair is used to represent the J/ψ, which necessarily emerges at $p_T = 0$. No J/ψ spin predictions are possible from the semilocal approach, and normalization is uncertain.

[5]The process $\gamma g \to c\bar{c}\, g$ is studied by D. W. Duke and J. F. Owens, Phys. Lett. 96B, 184 (1980), and by T. Tajima and T. Watanabe, Phys. Rev. D 23, 1517 (1981). However, these authors do not require the $c\bar{c}$ pair to be a color singlet, and they do not normalize to Γ^J_{ee}. Instead they use semilocal duality to obtain cross sections. Because we require that our $c\bar{c}$ pair be a color singlet, our set of order-g^2 diagrams also differs from that of Duke and Owens and Tajima and Watanabe; we have no diagram with a three-gluon vertex. Our amplitude is also infrared finite.

[6]T. H. Bauer, R. D. Spital, D. R. Yennie, and F. M. Pipkin, Rev. Mod. Phys. 50, 261 (1978).

[7]Consult, e.g., the review by V. A. Novikov, L. B. Okun, M. A. Shifman, A. I. Vainshtein, M. B. Voloshin, and V. I. Zakharov, Phys. Rep. 41C, 2 (1978); G. P. Lepage and S. J. Brodsky, Phys. Rev. D 22, 2157 (1980); E. L. Berger and S. J. Brodsky, Phys. Rev. Lett. 42, 940 (1979).

[8]W. Celmaster, Argonne Report No. ANL-HEP-CP-80-60, 1980 (unpublished) (talk presented at the XXth International Conference on High Energy Physics, Madison, Wisconsin, 1980).

[9]B. Gittelman *et al.*, Phys. Rev. Lett. 35, 1616 (1975); V. Camerini *et al.*, *ibid.* 35, 483 (1975); B. Knapp *et al.*, *ibid.* 34, 1040 (1975); T. Nash *et al.*, *ibid.* 36, 1233 (1976); A. R. Clark *et al.*, *ibid.* 43, 187 (1979); J. J. Aubert *et al.*, Phys. Lett. 89B, 267 (1980).

[10]J. J. Aubert *et al.*, CERN Report No. CERN-EP/80-84, 1980 (unpublished).

[11]G. R. Farrar, Nucl. Phys. B77, 429 (1974); J. F. Gunion, Phys. Rev. D 10, 242 (1974).

[12]A. R. Clark *et al.*, Phys. Rev. Lett. 45, 686 (1980).

[13]L. Lewin, *Dilogarithms and Associated Functions* (MacDonald, London, 1958).